Search for evidence of planets' migration based on mid-infrared spectroscopy of interplanetary dust emission with *AKARI*/IRC

Aoi Takahashi,[1,2] Hideo Matsuhara,[3,2] Takafumi Ootsubo,[2] Itsuki Sakon,[4] and Fumihiko Usui[5]

[1]*Department of Space and Astronautical Science, The Graduate University for Advanced Studies (SOKENDAI), Hayama 240-0193, Japan*

[2]*Institute of Space and Astronautical Science, Japan Aerospace Exploration Agency, 3-1-1 Yoshinodai, Chuo-ku, Sagamihara 252-5210, Japan*

[3]*Department of Space and Astronautical Science, The Graduate University for Advanced Studies (SOKENDAI), Shonan Village, Hayama 240-0193, Japan*

[4]*Graduate School of Science, The University of Tokyo, 7-3-1 Hongo, Bunkyo-ku, Tokyo 113-0033, Japan*

[5]*Center for Planetary Science, Graduate School of Science, Kobe University, 7-1-48 Minatojima-Minamimachi, Chuo-Ku, Kobe 650-0047, Japan*

ABSTRACT

The property of interplanetary dust (IPD), which has been recently emitted from planetesimals like asteroids and/or comets, can give us the information about the environment where asteroids and comets were formed during the planet-formation stage. These can include clues of any planetesimal scattering due to planets' migration. We use silicate features around 10 μm as a tracer of the thermal history. In this study, we analyze mid-infrared spectroscopic data of zodiacal emission at 74 different directions obtained with *AKARI*/IRC. After we examined and subtracted instrumental artifacts, we successfully obtained the high S/N spectra and detected the silicate feature in all pointing data. They also suggest the variations in dust temperature and shape of the feature among different ecliptic latitudes.

Keywords: Zodiacal emission, Interplanetary dust, Silicate feature

1. INTRODUCTION

In interplanetary space of our solar system, dust particles diffusely distribute and we call them "interplanetary dust (IPD)". Some dust detectors on board spacecrafts such as *Helios*, *Pioneer*, and *Ulysses* revealed their size distribution of sub-μm – cm with peak at $\sim$100 μm (Grün et al. 1985). They scatter and absorb the sunlight in UV to near-IR, and thermally re-radiate in mid- to far-IR as zodiacal emission. The spatial distribution of IPD was modeled using brightness distribution of zodiacal emission obtained by the Diffuse Infrared Background Experiment (DIRBE) on *the Cosmic Background Explorer* (*COBE*; Kelsall et al. 1998). The zodiacal emission spectra obtained by the Camera on Infrared Space Observatory (ISOCAM; Reach et al. 2003) and Mid-infrared Spectrometer (MIRS) on board *the Infrared Telescope in Space* (*IRTS*; Ootsubo et al. 1998) suggested the emission feature in the 9–11 μm, which originates from silicate.

IPD is thought to have been incorporated into planetesimals in the proto-solar system, and recently been emitted again from survived planetesimals like asteroids and/or comets. IPD's thermal history can give us any information where they have been incorporated and those planetesimals were formed during the planet-formation stage. The comparison of the information with current orbits of comets and asteroids can include clues of planetesimal scattering due to planets' migration (DeMeo et al. 2014). As one of the tracers of IPD's thermal history, we focused on silicate features around 10 μm in zodiacal emission spectra. The difference of environment IPD have experienced affect some properties of IPD and finally cause the different shape of these features.

In addition, IPD originating from different types of planetesimals distributes differently in ecliptic latitudes (elats). Some dynamical simulations show orbital evolutions of IPD after the emission from original planetesimals. They can reproduce the current distribution of IPD consistent with imaging observation data. According to them, IPD originating from comets distribute globally along all elats, with distribution peak near ecliptic plane (Nesvorný et al. 2010). On the other hand, IPD originating from asteroids exist in dust bands, which are seen locally in specific elats (Sykes et al. 1986).

Therefore, we investigated and compared silicate features in zodiacal emission spectra at various elats. In this paper, we show the derivation process and result of those silicate features, with their qualitative interpretation.

2. OBSERVATION AND DATA REDUCTION

Infrared Camera (IRC; Onaka et al. 2007) on *AKARI* (Murakami et al. 2007) has slit-spectroscopic observation mode for the spectroscopy of diffuse sources. We have performed near- and mid-infrared spectroscopic observation of zodiacal

emission with *AKARI*/IRC. In this study, we used the data obtained with the Mid-Infrared Short (MIR-S) channel, which covered 5–12 μm with a spectral resolution of $R \sim 50$, for investigation of silicate features around 10 μm. Thanks to the Sun-synchronous polar orbit, *AKARI* has a capability to observe the entire sky regions and it is suitable for the comparison among fields with different elats. We analyzed 74 pointing data obtained during the phase 2 (November 2006 – August 2007).

These spectroscopic data were taken with two grisms, SG1 (5.4–8.4 μm) and SG2 (7.5–12.9 μm), in the MIR-S channel. With conventional reduction (Ohyama et al. 2007), the resultant SG1 and SG2 spectra are not smoothly connected due to the inconsistency in the intensity level of the overlapping wavelength range (i.e., 7.5–8.4 μm). We have carefully investigated the properties of the possible artifacts in the spectroscopic data and have identified and quantitatively evaluated the following three artifacts that affect the slit-spectroscopic data:

Light scattered by the edge of the detector (see Appendix 1 in Sakon et al. 2007):
Aperture mask was common between the Near-Infrared (NIR) channel and the MIR-S channel. However, the field of view determined by the edge of the aperture mask is designed to be larger than that determined by the MIR-S detector's array. Therefore, a part of the incoming light through the aperture window for a point source spectroscopy in NIR channel are scattered by edge of the detector in MIR-S channel and produces photons that contaminate the slit spectroscopy region.

Light scattered on the detector surface (see Appendix 2 in Sakon et al. 2007):
On detector surface, certain fractions of the incoming light are scattered into pixels in the same row and column, even if they do not saturate. This component becomes the primary contamination in the slit spectroscopy region.

Ghost spectra from the aperture window:
A ghost component produced by the incoming light through the aperture window for NIR channel was recognized in the slit spectroscopy region.

We have empirically estimated their profiles common to all pointing data and calculated these absolute values from observed images for each pointing data. Finally, we succeeded to subtract these artifact components and derive to reasonable spectra smoothly connected between data in SG1 and SG2 for all pointing data. Their intensity levels are consistent with that predicted by the DIRBE's model (Kelsall et al. 1998).
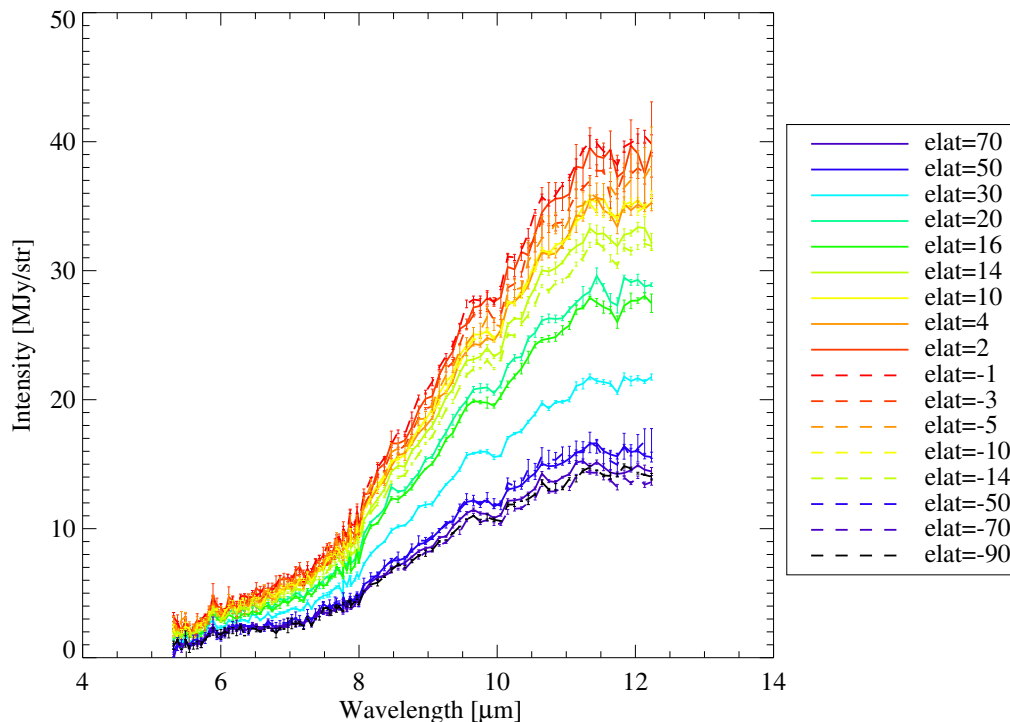

Figure 1. Zodiacal emission spectra scaled and averaged in each bin of ecliptic latitudes (elats). Each spectrum includes statistic errors of dispersion in the spatial direction and systematic errors of the response curve.

3. **RESULT**

We compared the shape of silicate features among the spectra with different elats. At first, we categorized all pointing data into 17 elat bins (< ±2° in a bin) and scaled each spectrum so that their intensities at 8 μm, 10 μm, and 12 μm match to mean intensities of all spectra in the same bin. After that, we averaged these scaled spectra in each elat bin. Figure 1 shows these averaged spectra. The error bars indicate the standard errors of the averaging in each elat bin. This averaging process enables us to obtain high S/N spectra and takes advantage of *AKARI*'s sky covering. As Figure 1, spectra averaged in lower elat bins have a stronger intensity than that of ecliptic poles, because more dust are included in the line of sight.

Against each averaged spectra, we fit a diluted black body of single temperature ($\tau B_\nu(T)$; τ and T mean the optical depth independent of wavelength and the dust temperature typical in the line of sight, respectively) as a continuum spectra. For the fitting, we used the data in 7.7–8.0 μm and 12.0–12.3 μm, which seems not to be contaminated by features. These best-fitted values are shown in Figure 2 as functions of elat. The main component of IPD distributes globally with a peak near ecliptic plane, which is consistent with past observations (Hauser et al. 1984). Therefore, lines of sight at lower elat include more IPD far from the Sun and best-fitted temperatures become lower at near ecliptic plane than ecliptic poles.

At the last step, We divided each spectrum by the fitted continuum and obtained emissivity spectra in each elat bin. We plot the emissivity spectra at elat −1°, 30° and 70° bins in Figure 3, which stand for that of low, middle and high elat, respectively. We can see excess emission of a few tens % above the diluted black body in all elat bins.
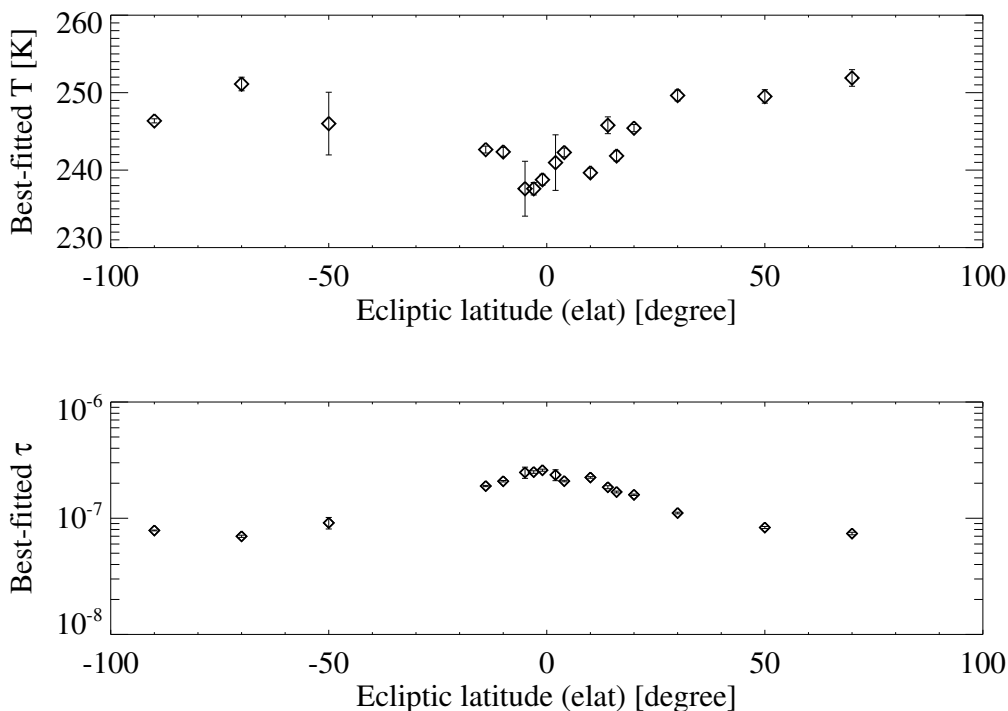

Figure 2. Best-fitted parameter for continuum fitting to a diluted black body in each bin of ecliptic latitudes (elats). Top: Best-fitted temperature (T), Bottom: Best-fitted optical depth (τ). The errors in elat −50°, −5° and 2° bins become large because only one pointing data is included in each bin and they cannot make use of the merit of averaging.

4. **DISCUSSION**

Emissivity spectra in all elat bins have some significant peaks. They are mainly by Si-O vibration mode in crystal silicates. Since the crystallization can occur only at the temperature higher than 800 K, IPD at all elat can be thought to have experienced environment with such high temperature. The peaks around 9.2, 9.5, 10.6, and 11.1 μm are contributed by crystal pyroxene (Chihara et al. 2002) and they are more significant at high elat, while peaks by crystal olivine around 10.2, 11.3, and 11.9 μm(Koike et al. 2003) are not so different. It indicates that olivine/pyroxene ratio is lower at high elat. In addition, our emissivity spectra show the comparable strength at 10.2 and 11.3 μm, although crystal olivine causes the main peak at 11.3 μm relatively much stronger than other peaks. It is quite likely that any compositions other than olivine or pyroxene are significantly contributed. One of the possible candidates is feldspar, another type of silicate (Chihara & Koike 2017). We can also find the peaks around 8.8 μm contributed by small (∼1 μm size) dust of quartz in all elat bins.
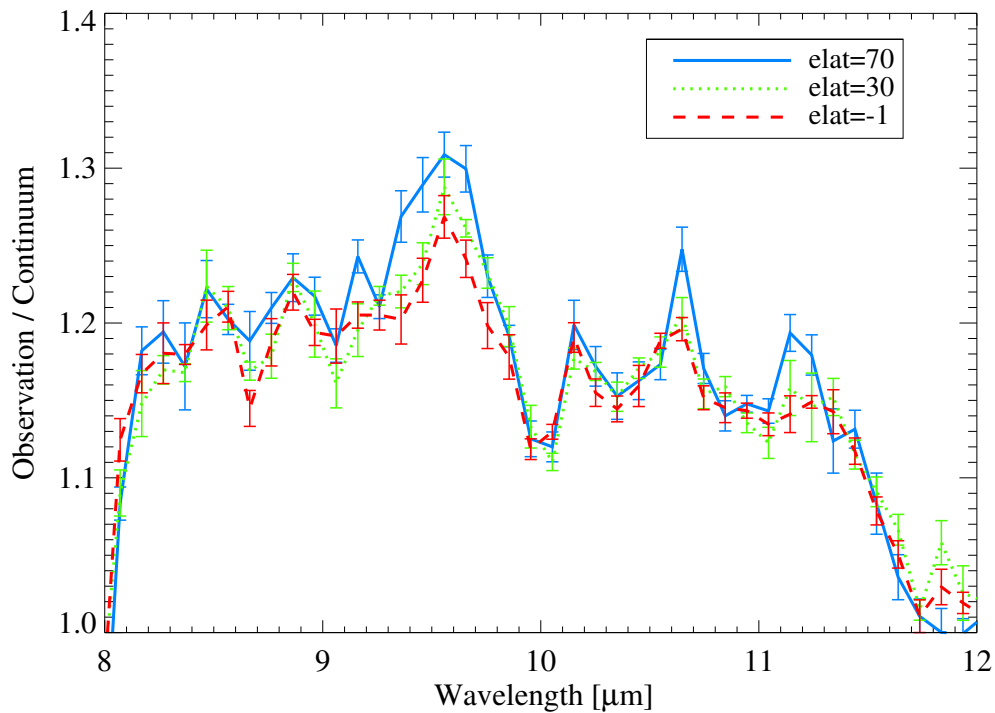
Figure 3. Emissivity spectra of zodiacal emission in −1°, 30° and 70° bins of ecliptic latitudes (elats).

5. SUMMARY

To investigate and compare the silicate features in zodiacal emission at various ecliptic latitudes, we used the data obtained by *AKARI*/IRC at 74 pointing directions. From the mid-infrared slit-spectroscopic data, we subtracted three instrumental artifacts and derived spectra. After averaging in near ecliptic latitudes and the continuum fitting, emissivity spectra in each ecliptic latitude bin were obtained. They indicate the contribution by crystal silicates and difference of olivine/pyroxene ratio among ecliptic latitudes.

REFERENCES

Chihara, H., Koike, C., Tsuchiyama, A., et al. 2002, A&A, 391, 267
Chihara, H., & Koike, C. 2017, Planet. Space Sci., 149, 94
DeMeo, F. E. and Carry, B. 2014, Nature, 505, 7485, 629
Grün, E., Zook, H. A., Fechtig, H., and Giese, R. H. 1985, Icarus, 62, 244
Hauser, M. G., Gillett, F. C., Low, F. J., et al. 1984, ApJ, 278, 15
Kelsall, T., Weiland, J. L., Franz, B. A., et al. 1998, ApJ, 508, 44
Koike, C., Chihara, H., Tsuchiyama, A., et al. 2003, A&A, 399, 1101
Murakami, H., Baba, H., Barthel, P., et al. 2007, PASJ, 59, S369
Nesvorný, D., Jenniskens, P., Levison, H. F., et al. 2010, ApJ, 713, 816
Ohyama, Y., Onaka, T., Matsuhara, H., et al. 2007, PASJ, 59, S411
Onaka, T., Matsuhara, H., Wada, T., et al. 2007, PASJ, 59, S401
Ootsubo, T., Onaka, T., Yamamura, I., et al. 1998, Earth Planets and Space, 50, 507
Reach, W. T., Morris, P., Boulanger, F., and Okumura, K. 2003, Icarus, 164, 2, 384
Sakon, I., Onaka, T., Wada, T., et al. 2007, PASJ, 59, S483
Sykes, M. V. and Greenberg, R. 1986, Icarus, 65, 51